Journal of Magnetism and Magnetic Materials 322 (2010) 315–321

Contents lists available at ScienceDirect

Journal of Magnetism and Magnetic Materials

journal homepage: www.elsevier.com/locate/jmmm

Transmission electron microscopy study of large field induced anisotropy $(Co_{1-x}Fe_x)_{89}Zr_7B_4$ nanocomposite ribbons with dilute Fe-contents

P.R. Ohodnicki Jr.[a,b,*], Y.L. Qin[a,b], M.E. McHenry[a,b], D.E. Laughlin[a], V. Keylin[b]

[a] Materials Science and Engineering Department, Carnegie Mellon University, Pittsburgh, PA 15213, USA
[b] Magnetics, A Division of Spang & Company, Pittsburgh, PA 15238, USA

ARTICLE INFO

Article history:
Received 3 April 2009
Received in revised form
21 July 2009
Available online 17 September 2009

PACS:
75.30.Gw
75.50.Tt
75.50.Bb

Keywords:
Induced magnetic anisotropy
Stacking fault
CoFe
Nanocrystalline
Amorphous
fcc
hcp

ABSTRACT

Electron microscopy was employed to investigate the structure of magnetic field crystallized $(Co_{1-x}Fe_x)_{89}Zr_7B_4$ alloys with only dilute Fe-contents (x=0, 0.025, 0.05, and 0.10). The x=0.025 and 0.05 alloys exhibit very large field induced anisotropies and multiple nanocrystalline phases (BCC, FCC, and HCP) surrounded by an intergranular amorphous phase. Correlation between the volume fraction crystallized and the measured value of H_K suggests that the large K_U values are associated with the crystalline phases that form. Multiple crystalline phases are present for the highest K_U alloys and so the presence of FCC and/or HCP-type nanocrystals may be responsible for these observations. High-resolution transmission electron microscopy (HRTEM) illustrates a number of microstructural features including (1) high densities of stacking faults in many of the FCC and, in particular, the HCP-type nanocrystals, (2) infrequent BCC/FCC orientation relationships, and (3) nanocrystals with disordered or long period stacking sequences of close-packed planes. High densities of planar faults are suggested as a potential source of K_U for the FCC and HCP-type nanocrystals, but the origin of the large values of K_U found in dilute Fe-containing, Co-rich "nanocomposite" alloys is an area where further work is needed.

1. Introduction

Co-rich Co,Fe-based nanocrystalline and amorphous "nanocomposites" are interesting because of the similar free energies of BCC, FCC, and HCP crystalline phases [1,2] as well as their relatively large responses to magnetic field annealing processing [2–4]. Previous work on Co-rich nanocomposites of composition $(Co,Fe)_{78.8}Nb_{2.6}Si_9B_9Cu_{0.6}$ and $(Co,Fe)_{78.8}Zr_{2.6}Si_9B_9Cu_{0.6}$ has demonstrated a large field induced anisotropy, K_U, and low core losses for Fe:(Fe+Co) ratios ranging between approximately 0.10–0.20 [3,4]. For these alloys, the high K_U compositions contained only a BCC nanocrystalline phase surrounded by an intergranular amorphous matrix after crystallization. A number of other Co-rich compositions with high field induced anisotropies are listed in a relatively recent patent [5].

In our work, we have investigated the phase evolution and field induced magnetic anisotropy in the $(Co_{1-x}Fe_x)_{89}Zr_7B_4$ and $(Co_{1-x}Fe_x)_{88}Zr_7B_4Cu_1$ systems. Alloys of varying Fe:Co ratio spanning the entire composition range were synthesized and subjected to field annealing experiments [2]. Relatively large K_U values were observed for Co-rich alloys as in previously studied systems [3,4]. With the exception of dilute Fe-containing (x=0.025, 0.05) or Fe-free (x=0) alloys that exhibited multiple crystalline phases after crystallization (BCC, FCC, HCP) and relatively large values of K_U, the observed trends in K_U could be rationalized in terms of directional ordering models [2]. For the highest Co-containing alloys with multiple crystalline phases, however, the large K_U values are suggestive that another mechanism may be active. In the interest of brevity, the reader is referred to our previous works for a thorough discussion of the compositional dependence of K_U in these systems [2]. The work described here focuses primarily on a detailed transmission electron microscopy study of the microstructure and phase identity of the high K_U samples and an attempt to gain more insight into possible microstructural mechanisms. Based on these results, some potential sources of the large measured values of K_U are discussed briefly. Note that some of the results for the Fe-free $Co_{89}Zr_7B_4$ composition were presented previously [6].

2. Experimental procedure

Co-based amorphous ribbons of composition $(Co_{1-x}Fe_x)_{89}Zr_7B_4$ with x=0.00, 0.025, 0.05, and 0.10 were synthesized by arc-melting

* Corresponding author at: Materials Science and Engineering Department, Carnegie Mellon University, Pittsburgh, PA 15213, USA.
E-mail address: paul.ohodnicki@gmail.com (P.R. Ohodnicki Jr.).

0304-8853/$ - see front matter © 2009 Elsevier B.V. All rights reserved.
doi:10.1016/j.jmmm.2009.09.047

techniques to obtain ingots of the appropriate composition followed by rapid solidification through melt-spinning processing. The ribbons were wound into toroidal cores and annealed for 1 h in a 2 T magnetic field applied transverse to the long axis of the ribbon at Magnetics, A Division of Spang and Company. A number of different annealing temperatures were chosen to lie significantly below and above the primary crystallization temperature of these alloys. The field induced magnetic anisotropy, K_U, was estimated using AC permeametry of toroidal tape-wound cores of the synthesized ribbons. The phase identity and microstructure of the ribbons were investigated using X-ray diffraction (XRD) with a Philips X'pert thin film diffractometer and conventional transmission electron microscopy (CTEM) using a JEOL 2000 TEM. More detailed investigation of the microstructure was performed using high-resolution transmission electron microscopy (HRTEM) of selected alloys with a Tecnai F20.

3. Experimental results and discussion

In Fig. 1a, the compositional trend of field induced anisotropy, K_U, for the $(Co_{1-x}Fe_x)_{89}Zr_7B_4$ alloys is presented for two different field annealing temperatures. For T_{Anneal}=350 °C, XRD patterns obtained from the side of the ribbon in contact with the cooling wheel show only broad intensities characteristic of amorphous metals. Such ribbons are therefore referred to as "field annealed amorphous". For T_{Anneal}=540 °C, XRD peak intensity associated with the formation of a significant volume fraction of nanocrystals is observed. Ribbons field annealed at temperatures sufficiently high for crystallization to take place are referred to as "field crystallized". For the field annealed amorphous ribbons of Fig. 1a it is observed that the value of K_U increases monotonically with increasing Fe-content as would be expected for directional pair ordering of Fe and Co atoms [2]. For the field crystallized alloys, however, a peak in K_U is observed for the x=0.05 and 0.025 alloys for which evidence of multiple nanocrystalline phases are found in the XRD data of Fig. 1b. According to the X-ray data presented, the following phases can be unambiguously identified in each sample: BCC for x=0.10, BCC and FCC for x=0.05, BCC, FCC, and HCP for x=0.025, and FCC and HCP for x=0. The correspondence between the large measured values of K_U and the formation of FCC and/or HCP-type nanocrystals for the high K_U compositions suggest that one or both of these phases may be responsible for the large field annealing response.

At this point, it is important to note that compositional partitioning upon crystallization complicates any comparison of trends in properties with the composition of individual phases in the nanocomposite microstructure. These complications were demonstrated most recently for alloys similar to those under investigation here and it appears that the composition of the BCC crystallites, FCC/HCP crystallites, and the amorphous phase all deviate from the nominal alloy composition [2]. Because these complications are not thought to impact the conclusions of the present study, the reader is referred to the previous work for a more detailed discussion of compositional partitioning effects in these alloys.

A quantitative estimate of the relative volume fraction of each phase is difficult to obtain because of the broad XRD peaks. It is also impossible to exclude the possibility of a minor amount of a phase that cannot be detected in the XRD data. Nevertheless, it can be concluded that there is no direct correlation between the relative volume fraction of a particular crystalline phase and the value of K_U because the largest values of K_U are measured for the x=0.025 and 0.05 alloys when significant amounts of all three phases are present. Therefore, if the large values of K_U are primarily associated with the FCC and/or HCP nanocrystals in these alloys, the compositional dependence illustrated in Fig. 1a could only be explained by a dramatic increase in K_U of the FCC and/or HCP nanocrystals with dilute additions of Fe.

In Fig. 1a, the anisotropy fields, H_K, estimated from B–H loops obtained at f=3 kHz are presented for the same alloys for a number of different field annealing temperatures. The values of H_K were obtained by extrapolating the low field linear portion of the B–H loop to the saturation induction. Because the saturation magnetization of the as-cast amorphous and crystallized ribbons are similar for the highest Co-containing alloys, the field induced anisotropy constant estimated using $K_U=(H_K M_S)/2$ exhibits a similar annealing temperature dependence as H_K. The vertical arrows indicate the approximate temperature ($T\sim$450 °C) at which the first peaks associated with formation of a nanocrystalline phase or phases can be identified through standard X-ray diffraction (XRD) techniques after the field annealing treatment. Therefore, this temperature serves as the boundary between the annealing temperatures at which the annealed ribbons are considered field crystallized or field annealed amorphous in the plots of Fig. 1. For the x=0.025 and 0.05 alloys, a large increase in H_K is observed at annealing temperatures sufficiently high for crystallization to occur suggesting that the large values of K_U are associated with the crystalline phases that form.

The correspondence between crystallization and the formation of large values of K_U is more clearly illustrated by comparison of an estimate of the relative crystal volume fraction presented in Fig. 2b with the measured H_K values presented in Fig. 2a. These estimates were obtained using bright field images, portions of which are presented in Fig. 3a and b. The true volume fraction crystallized is very difficult to estimate using electron microscopy techniques because of the possibility of small grain sizes relative

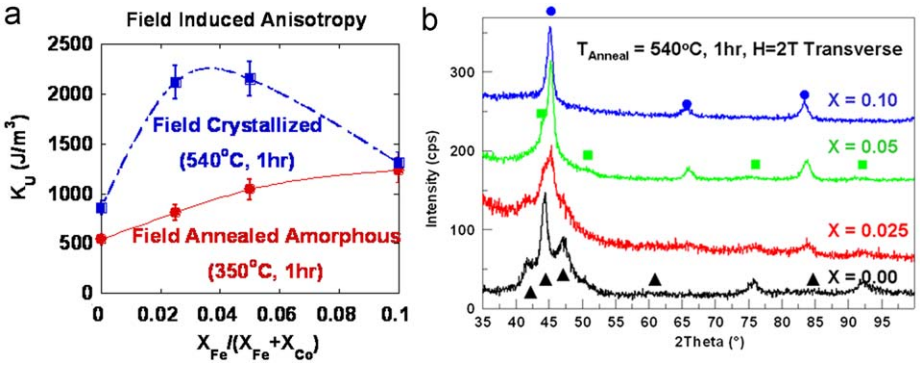

Fig. 1. (a) Field induced anisotropy, K_U, estimated from dynamic B–H loops with f=3 kHz for field annealed amorphous (T_{Anneal}=350 °C) and field crystallized (T_{Anneal}=540 °C) $(Co_{1-x}Fe_x)_{89}Zr_7B_4$ alloys. (b) X-ray diffraction data obtained from the field crystallized alloys (T_{Anneal}=540 °C) illustrating peaks associated with various crystalline phases including BCC (circles), FCC (squares), and HCP (triangles).

to the foil thickness. The relative crystal volume fraction presented in Fig. 2b is defined as the estimated areal density of crystalline phase for each annealing temperature relative to the maximum estimate of the areal density for the T_{Anneal}=540 °C samples. The error bars were obtained by maximum and minimum estimates of areal density for each annealing temperature. We note that some nanocrystals were observed to be present in the as-cast ribbons as illustrated in Fig. 3 even though XRD provides no evidence of crystalline phase. In some regions of the ribbons, clusters of grains have even been observed.

Comparison of Fig. 2b with Fig. 2a demonstrates that H_K correlates well with the relative crystal volume fraction for the x=0.025 alloy. For the x=0.05 alloy, an experimentally significant increase in H_K is not observed for T_{Anneal}=450 °C despite an increase in the volume fraction crystallized. However, at higher annealing temperatures the value of H_K does increase for this composition. The discrepancy between these two samples for T_{Anneal}=450 °C could be due to a relatively low volume fraction of FCC and HCP phases for the x=0.05 sample that increases for the higher annealing temperature treatments. Although this trend is suggested in selected area diffraction patterns (SAD) not presented here [2], it is difficult to show conclusively. In any case, the overall correlation between the values of H_K and the volume fraction crystallized for both samples is reasonable evidence that the high H_K values are due primarily to the crystalline phases that form upon crystallization. A similar conclusion was arrived at for the high K_U alloys of the $(Co,Fe)_{78.8}Nb_{2.6}Si_9B_9Cu_{0.6}$ and $(Co,Fe)_{78.8}Zr_{2.6}Si_9B_9Cu_{0.6}$ systems [3,4].

For the higher Fe-containing alloys with only a BCC nanocrystalline phase after crystallization, the measured compositional dependence of K_U has been discussed in terms of directional pair ordering of Fe and Co atoms in both the crystalline and amorphous phase and some additional contributions that are presumably due to the presence of Zr and B [2,7]. For the high Co-containing alloys investigated here, the same mechanisms are expected to be active as well and it is possible that these effects result in larger values of K_U for the FCC and HCP phases as compared to the BCC phase. However, there is also the possibility of additional microstructural mechanisms active for the FCC and HCP phase that are not active in the BCC phase. The potential sources of such microstructural mechanisms include crystallographic texture or planar defects which were suggested as possible sources of K_U in previous work on bulk Co-rich Co–Ni crystalline alloys subject to field annealing in order to undergo martensitic transformations between the FCC and HCP phases [8]. No evidence for such martensitic transformations has been observed for these "nanocomposite" alloys [6], but similar arguments could be made for field crystallization of these phases

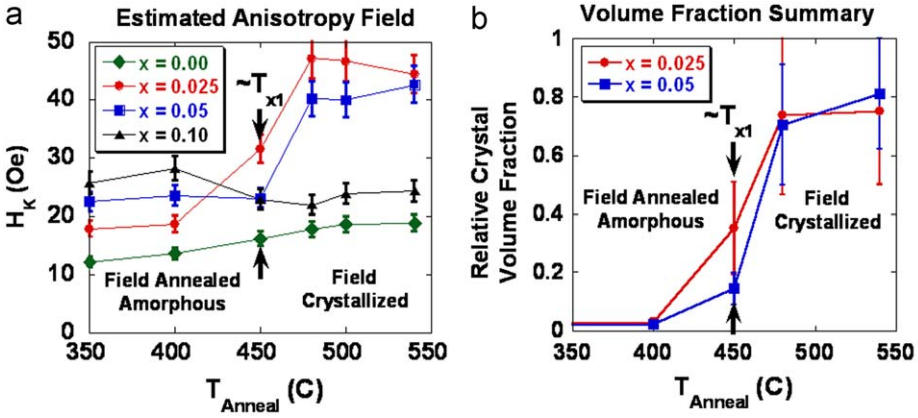

Fig. 2. (a) Estimated anisotropy fields from dynamic B–H loops at f=3 kHz for $(Co_{1-x}Fe_x)_{89}Zr_7B_4$ alloys as a function of annealing temperature. (b) Estimates of relative crystal volume fraction based on bright field images presented in Fig. 3. The relative crystal volume fraction is defined in the text and the error bars in (b) represent maximum and minimum estimates. The vertical arrows indicate the lowest annealing temperature at which X-ray diffraction measurements provide evidence for a significant volume fraction of a nanocrystalline phase or phases.

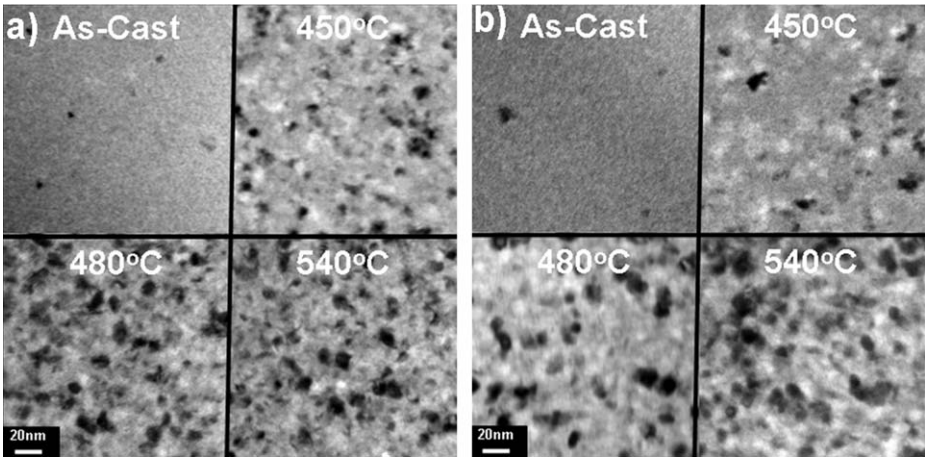

Fig. 3. Bright field images obtained for the (a) $(Co_{0.975}Fe_{0.025})_{89}Zr_7B_4$ and (b) $(Co_{0.95}Fe_{0.05})_{89}Zr_7B_4$ ribbons as-cast and after transverse field annealing at several different temperatures as indicated on the image.

from an amorphous precursor. Particularly relevant to the alloys under investigation here, stacking faults have been proposed as the source of magnetic anisotropy observed after plastic deformation of FCC-based dilute Fe-containing bulk Co–Fe alloys [9]. In the interest of brevity, the reader is referred to previous works for a discussion of stacking faults as a potential source of field induced anisotropy [8,9].

In light of a possible microstructural mechanism for the large values of K_U in the alloys studied here, we have performed a more detailed microstructural study of the field crystallized alloys annealed at T_{Anneal}=540 °C. In Fig. 4, the bright field images obtained using CTEM for all four samples are presented. These results suggest that the FCC and HCP containing x=0.00 alloy exhibits a reduced average grain size as compared to the BCC containing x=0.10 alloy. In Fig. 5a and b, the corresponding SAD patterns and circularly integrated intensity profiles are presented.

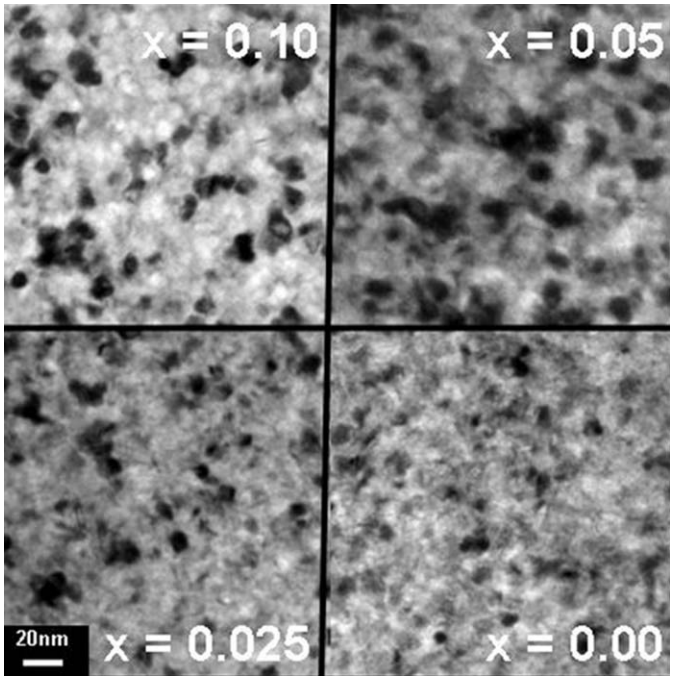

Fig. 4. Conventional transmission electron microscopy (CTEM) bright field images for the four Co-rich $(Co_{1-x}Fe_x)_{89}Zr_7B_4$ samples investigated in this work after transverse magnetic field crystallization at 540 °C for 1 h.

The phases identified from the SAD patterns are consistent with the conclusions derived from the corresponding XRD data of Fig. 1b. In SAD patterns obtained, we have not found experimentally significant evidence for in-plane crystallographic texture of any of the phases. It is also well known that the easy axis of HCP Co switches from the c-axis to the basal plane for temperatures greater than approximately 250 °C so that development of crystallographic texture during field crystallization experiments would actually induce a hard axis along the annealing field direction at room temperature rather than an easy axis [6]. Therefore, formation of crystallographic texture is not a likely mechanism responsible for the large values of K_U measured for the dilute Fe-containing alloys investigated here.

Because planar defects such as stacking faults have also been proposed as a possible source of induced anisotropy in previously studied Co-rich alloys [8,9], high-resolution transmission electron microscopy (HRTEM) was performed on selected field crystallized samples (T_{Anneal}=540 °C) to more carefully probe the microstructure of these multi-phase nanocomposites.

In Fig. 6, the HRTEM image of a nanocrystalline grain with a high density of stacking faults is presented for the x=0.00 $Co_{89}Zr_7B_4$ sample. The overall fast Fourier transform (FFT) of the grain presented in Fig. 6c is best described as a $[1\,1\,0]_{hcp}$ zone axis pattern with streaking along the normal of the close-packed planes, $[0\,0\,1]_{hcp}$, due to the presence of stacking faults. However, for the FFT's taken from regions labeled 1 and 2 in Fig. 6c, it can be seen that these regions of the grain exhibit diffraction patterns that more closely resemble faulted $[1\,1\,0]_{hcp}$ or $[1\,1\,0]_{fcc}$-type zone axis patterns, respectively. Because the only difference between the FCC and HCP structures is the stacking sequence of the close-packed planes, the high density of stacking faults can result in local regions of FCC- or HCP-type stacking or even regions of disordered stacking sequences that cannot be clearly indexed to either phase. The highly faulted nature of grains that are classified as "HCP" type based on the overall FFT is the expected source of the relatively broad, weak intensities of the peaks indexed to the HCP phase in the XRD and CTEM results presented above.

In Fig. 7, HRTEM results from the x=0.05 $(Co_{0.95}Fe_{0.05})_{89}Zr_7B_4$ sample field annealed at 540 °C are presented illustrating a BCC (Fig. 7a) and an FCC (Fig. 7b) grain that do not contain any planar defects, as well as an "HCP" grain with stacking faults that are once again identified by the presence of streaking along $[0\,0\,1]_{hcp}$ in the corresponding FFT (Fig. 7c). Although HCP peaks are weak and often difficult to identify in the CTEM and XRD data presented above for this sample, we find clear evidence for this phase in the HRTEM data. In general, the grains that can be identified as

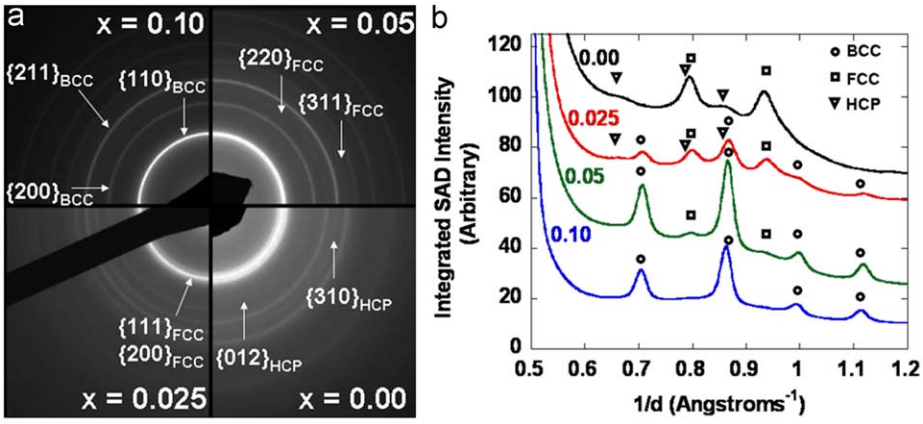

Fig. 5. (a) Selected area diffraction patterns for the four Co-rich $(Co_{1-x}Fe_x)_{89}Zr_7B_4$ samples investigated in this work after transverse magnetic field crystallization at 540 °C for 1 h. (b) Circularly integrated intensity profiles of the selected area diffraction patterns. Only selected rings are labeled in the selected area diffraction patterns of (a) and only peaks that can unambiguously be identified are labeled in (b). The peak observed for $1/d \sim 0.5$ (angstroms^{-1}) corresponding to the innermost ring of (a) is not included in (b).

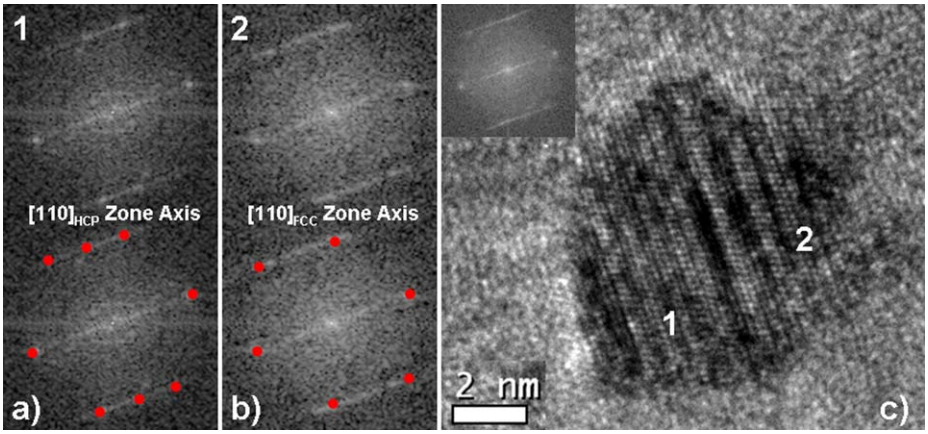

Fig. 6. HRTEM Image for the x=0.00 sample field annealed at 540 °C that is classified as a faulted HCP grain based on the overall FFT presented in (c). FFT's from selected regions of the grain indicate regions where the stacking sequences more closely resemble HCP (a) or FCC (b).

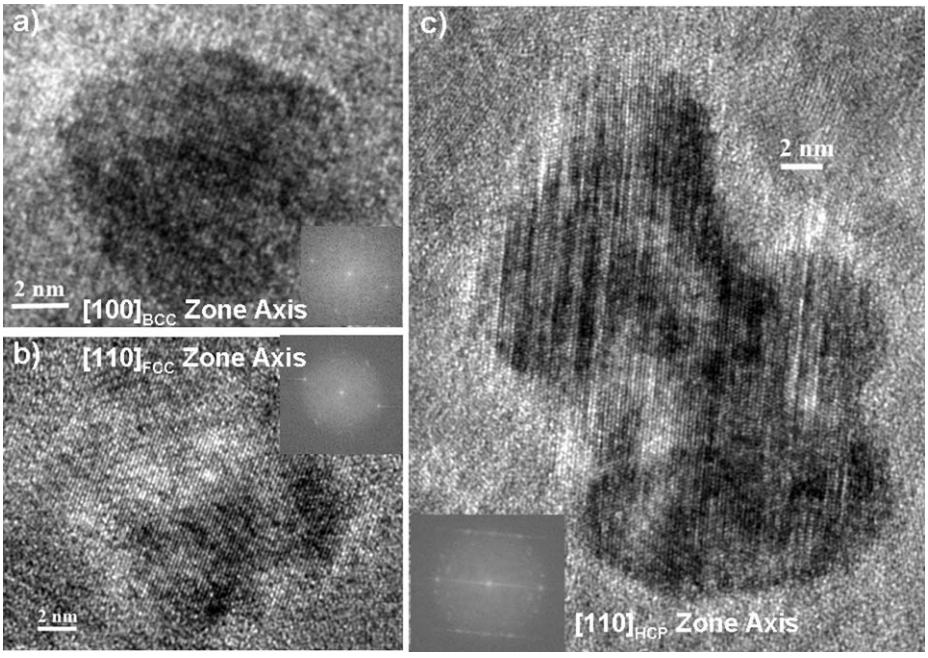

Fig. 7. HRTEM Images for the x=0.05 sample field annealed at 540 °C indicating (a) a BCC grain, (b) an FCC grain, and (c) a highly faulted HCP grain.

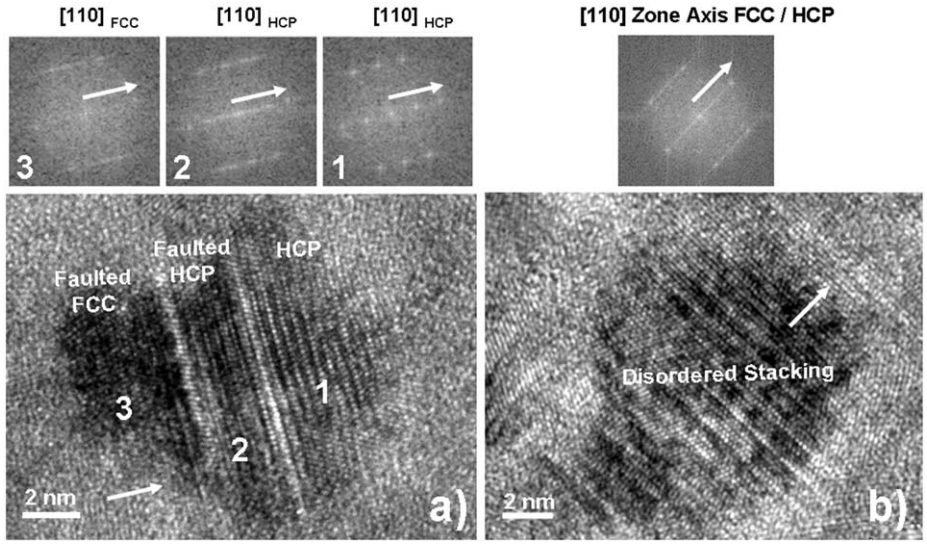

Fig. 8. HRTEM Images for the x=0.025 sample field annealed at 540 °C for which significant amounts of BCC, FCC, and HCP are all identified from XRD and CTEM. (a) A single nanocrystalline grain with a region of HCP (1), faulted HCP (2), and faulted FCC (3) according to the FFT's from each region presented above the image. (b) A grain with a disordered stacking sequence of close-packed planes such that the overall FFT cannot be indexed as FCC or HCP.

primarily HCP phase based on FFT's tend to exhibit a significant number of planar defects while the BCC nanocrystals are typically free of planar defects. Therefore, high densities of planar defects observed in many of the FCC/HCP-type nanocrystals could potentially provide an additional source of K_U relative to the BCC nanocrystals.

Because the BCC, FCC, and HCP phases are all present in significant amounts for the high field induced anisotropy $x=0.025$ $(Co_{0.975}Fe_{0.025})_{89}Zr_7B_4$ sample based on the XRD and CTEM results above, HRTEM investigations have been focused on this composition. In Fig. 8a, an FCC/HCP grain is shown in which three different regions are observed based on the FFT's obtained. Region 1 corresponds to a region of perfect HCP stacking, region 2 corresponds to a region that is classified as faulted HCP, and region 3 is classified as faulted FCC. In Fig. 8b, the stacking sequence of close-packed planes is disordered and the overall FFT cannot be clearly indexed as an FCC or HCP pattern. The normal of the close-packed planes corresponding to $[0\,0\,1]_{hcp}$ or $[1\,1\,1]_{fcc}$ for all of these images are indicated by the orientation of the arrows.

In addition to FCC (ABC stacking) and HCP (AB stacking), longer period stacking sequences of close-packed planes for pure Co or Co–Fe alloys with only dilute amounts of Fe have been observed previously. Examples include the double HCP structure (ABAC) [10] as well as a longer period 9R structure observed previously in fine particles [11]. The longer period stacking sequences exhibit a larger number of diffraction spots because of the higher d-spacings. In Fig. 9 we have identified a small region of longer period stacking in a nanocrystal as evidenced by the FFT obtained from this region. As in previous images, the normal to the close-packed planes is labeled by the arrow in the FFT. The stacking sequence appears to be the 9R structure based on the HRTEM image.

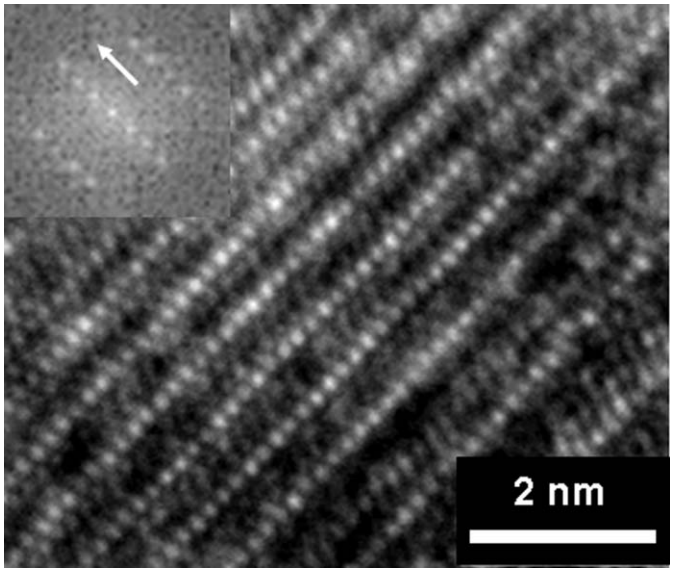

Fig. 9. HRTEM Image for the $x=0.025$ sample field annealed at 540 °C that shows a small region of a long-period stacking of close-packed planes in a nanocrystal and an accompanying FFT. The orientation of the normal of the close-packed planes is indicated by the arrow in the FFT. The stacking sequence appears to be the 9R structure.

For the $(Co_{0.975}Fe_{0.025})_{89}Zr_7B_4$ sample annealed at $T=540$ °C, evidence of {1 1 1}-type twins in regions with FCC stacking for the $(Co_{0.975}Fe_{0.025})_{89}Zr_7B_4$ sample have been observed. We have also observed evidence of nanocrystalline regions with orientation relationships. In Fig. 10, we present evidence for an orientation relationship between BCC and FCC nanocrystalline regions. In this case, the orientation relationship appears to be $(0\,0\,1)_{bcc}\|(1\,1\,0)_{fcc}$ and $[1\,1\,0]_{bcc}$ misoriented by approximately 3–6° with respect to $[1\,\bar{1}\,1]_{fcc}$. The FCC phase is expected to be more stable than BCC for bulk binary Fe,Co alloys with the same Co:Fe ratios. Such orientation relationships suggest that BCC nanocrystals may promote formation of FCC and possibly HCP phases by acting as heterogeneous nucleation sites or through direct transformation. However, the observation of orientation relationships between different phases is infrequent and so the majority of the FCC and HCP regions are thought to form without assistance from previously nucleated BCC nanocrystals.

The HRTEM results discussed here demonstrate that a large number of planar defects are observed using HRTEM for many nanocrystals classified as "FCC" and, especially, "HCP"-type based on XRD and CTEM while the BCC nanocrystals are typically free of planar defects. These defects could potentially provide an additional contribution to the K_U resulting in large values of K_U measured for the dilute Fe-containing $(Co_{1-x}Fe_x)_{89}Zr_7B_4$ alloys.

At this point, it is important to note that in the $(Co,Fe)_{78.8}Nb_{2.6}Si_9B_9Cu_{0.6}$ and $(Co,Fe)_{78.8}Zr_{2.6}Si_9B_9Cu_{0.6}$ alloys for which a peak in field induced anisotropy was first reported for the Co-rich nanocomposites [3,4], large values of K_U of similar magnitude were observed for alloys in which only a BCC crystalline phase was observed after crystallization. Therefore, the large magnitude of K_U observed in the previously investigated alloys can not be related to the presence of multiple nanocrystalline phases or high densities of stacking faults. We cannot say if the same mechanism of K_U is responsible for the large values of K_U in these previously investigated Si-containing alloys as the dilute Fe-containing $(Co_{1-x}Fe_x)_{89}Zr_7B_4$ alloys investigated here. Nevertheless, the previous work does raise doubts regarding the need for a direct link between the phase identity/microstructural observations and the large values of K_U in such alloys.

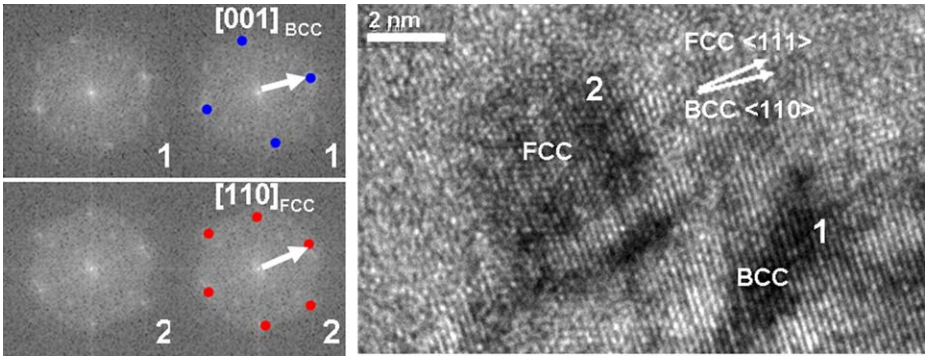

Fig. 10. Orientation relationship between a BCC (region 1) and FCC (region 2) nanocrystalline region with $(0\,0\,1)_{bcc}\|(1\,1\,0)_{fcc}$ and $[1\,1\,0]_{bcc}$ misoriented by approximately 3–6° with respect to $[1\,\bar{1}\,1]_{fcc}$. The normals of the closest-packed planes in the BCC and FCC regions are illustrated by a white arrow in the FFT's and they are only slightly misoriented with respect to one another as shown in the HRTEM image.

4. Conclusions

A correspondence between large field induced anisotropies and the presence of multiple nanocrystalline phases (BCC, FCC, and HCP) was observed for field crystallized $(Co_{1-x}Fe_x)_{89}Zr_7B_4$ alloys with only dilute Fe-contents (x=0.025 and 0.05). The observed correlation between the volume fraction crystallized and the measured value of H_K suggests that the large K_U is associated with the crystalline phases that form. Because they are only found in alloys with multiple nanocrystalline phases, the large values of K_U could be associated with the FCC and/or the HCP-type nanocrystals. However, the lack of a direct correlation between the volume fraction of a particular phase and the measured value of K_U requires that K_U of the FCC and/or HCP-type nanocrystals would necessarily increase dramatically with small Fe-additions to account for the observed compositional dependence of K_U in these systems.

A detailed microstructural investigation was performed using HRTEM and it highlighted the following:

(1) A high density of planar defects is found in many of the FCC and, especially, the HCP-type nanocrystals as identified based on the overall fast Fourier transform obtained from each grain. The vast majority of BCC nanocrystals exhibited no planar defects.
(2) An infrequent number of nanocrystalline regions such as BCC and FCC with orientation relationships were observed.
(3) Nanocrystals were found that cannot be clearly indexed as FCC or HCP-type due to disordered or longer period stacking sequences of close-packed planes.

High densities of stacking faults are therefore one potential source of relatively large values of K_U in these alloys. Nevertheless, further work is required in order to unambiguously identify the mechanisms responsible for the large values of K_U obtainable in the Co-rich "nanocomposite" alloys.

Acknowledgements

The authors gratefully acknowledge M.A. Willard of the Naval Research Laboratories for helpful discussions relevant to the work described here. P.R.O. acknowledges support from a National Defense Science and Engineering Graduate Research Fellowship throughout the preparation of this manuscript. Funding from the National Science Foundation is also acknowledged (NSF Grant #DMR-0406220).

References

[1] M. Willard, T. Heil, R. Goswami, Metallurgical and Materials Transactions A 38 (2007) 725–731.
[2] P.R. Ohodnicki, Ph.D. Thesis, Materials Science and Engineering Department, Carnegie Mellon University, 2008;
P.R. Ohodnicki Jr., Y.L. Qin, D.E. Laughlin, M.E. McHenry, M. Kodzuka, T. Ohkubo, K. Hono, M.A. Willard, Acta Materialia 57 (1) (2009) 87–96;
P.R. Ohodnicki Jr., J. Long, D.E. Laughlin, M.E. McHenry, V. Keylin, J. Huth, Journal of Applied Physics 104 (2008) 113909.
[3] S.F.Y. Yoshizawa, D.H. Ping, M. Ohnuma, K. Hono, Scripta Materialia 48 (2003) 863–868.
[4] S.F.Y. Yoshizawa, D.H. Ping, M. Ohnuma, K. Hono, Materials Science and Engineering A 375–377 (2004) 207–212.
[5] Y. Yoshizawa; US Patent: 6648990 B2, 2003.
[6] J.P.R. Ohodnicki, V. Keylin, H.K. McWilliams, D.E. Laughlin, M.E. McHenry, Journal of Applied Physics 103 (2008) 07E740-3.
[7] K. Suzuki, N. Ito, J.S. Garitaonandia, J.D. Cashion, Journal of Applied Physics 99 (2006) 08F114.
[8] M. Takahashi, T. Kono, Japanese Journal of Applied Physics 17 (1978) 361–369.
[9] L.M. Sandler, Y.V. Naglyuk, I.K. Zasimchuk, Y.L. Zhibolub, Physics of Metals and Metallography 53 (1982) 191–193.
[10] D. Balzar, A. Bonefacic, Journal of Materials Science 25 (1990) 1040–1042.
[11] S. Kajiwara, S. Ohno, K. Honma, M. Uda, Philosophical Magazine Letters 55 (1987) 215–219.